DOI: 10.31534/engmod.2023.2.ri.01m
Original scientific paper
Received: 15.02.2023.

On the Theory of Contact-induced Standing Waves in Rotating Tyres

Ivo Senjanović, Damjan Čakmak, Neven Alujević, Nikola Vladimir, Ivan Ćatipović

University of Zagreb, Faculty of Mechanical Engineering and Naval Architecture, Ivana Lučića 5, 10 002 Zagreb, CROATIA
e-mail: ivo.senjanovic@fsb.hr

SUMMARY

A new theory of contact-induced standing waves in rotating tyres is presented. The tyre is run by a rotating drum with a fixed shaft distance as in experiments. The tyre belt is modelled as a rotating ring whereas its sidewalls are modelled via radial stiffness of an elastic foundation supporting the ring. The differential equation of vibrations is reduced to the radial deflection of the ring. Critical rotation speed depends on the inflation pressure and the ring bending stiffness. Different tyre response functions are defined in the rotation speed domain with respect to the critical speed. The contact region between the tyre and the drum is defined considering the increase of the tyre radius due to the centrifugal load. Appropriate boundary conditions are specified in order to ensure a continuity of the ring deformation. Bearing reaction forces, as a result of drum penetration into the tyre, are defined.

KEY WORDS: *Tyre-drum system; ring model; boundary conditions; standing waves; analytical solution.*

1. INTRODUCTION

The standing waves phenomenon is observed in rolling tyres when the tyre rotation speed exceeds a certain critical value. Standing waves are stationary for an observer from a fixed ground point. However, a tyre particle rides on standing waves while the tyre actually vibrates in the moving coordinate system. The large deformation of the tyre surface due to the generation of standing waves induces a large amount of energy into the tyre material. This may cause a quick overheating of the tyre and its corresponding failure. Hence, the critical tyre rotation speed represents a significant performance limitation for high-speed vehicles.

The standing waves phenomenon has been investigated since the 1950s for traffic security reasons. A review of early theoretical and experimental studies until 1970 is presented in [1]. There have been many attempts for mathematical modelling of the standing waves phenomenon. Tyre models are commonly simplified starting from ring [2]-[10] to toroidal membrane approximation [11], thin cylindrical shell [12] and thin toroidal shell simplification [13]. Recently, the analogy of the ring model to the model considering a beam on elastic support has been used for the investigation of tyre standing waves, [14].

The development of standing waves has been interpreted in terms of a shock at the leading contact edge, in terms of resonance with natural vibrations, as well as a loss of dynamic stability. These interpretations are discussed in [7]. Experimental investigations have been performed on a test bed where the tyre has been driven by a rotating drum [7]. Insightful results were obtained and this reference is often cited in the literature.

Even relatively simple analytical models help to understand the fundamentals of the occurrence of tyre standing waves. However, their accuracy and applicability are not satisfactory due to the complex tyre geometry, composite tyre materials and inherent geometrical and material nonlinearity. Therefore, an evident advantage of the finite element method (FEM) has been commonly exploited for tyre design purposes [15]-[22]. The reliability of the FEM analyses is evaluated via experiments [23].

In order to better understand the physical mechanisms responsible for the generation of tyre standing waves and the influence of different tyre parameters, in this paper a new mathematical model is presented by utilizing the ring vibration theory. The tyre belt is modelled as a ring, whereas the influence of sidewalls is simulated by an elastic foundation modelled as a distributed radial stiffness. Only the radial displacement, resulting from the centrifugal load, is taken into account since it is dominant when compared to the circumferential displacement. The problem is analysed in the fixed coordinate system. A general solution of the differential equation of motion is given. Different tyre responses are obtained depending on the ratio of the rotation speed and the critical speed, as well as the inflation pressure. The problem of tyre run by a rotating drum is analysed. The contact region is determined with appropriate boundary conditions to ensure the deformation continuity. In addition, reaction forces in the tyre and drum bearings are determined.

The paper is structured into 8 sections. In the introductory section, a short state-of-the-art in the field of the standing waves phenomenon has been summarized. In the second section, a simplified differential equation for ring vibration is given for stationary standing wave analysis. Section 3 deals with the solution of the differential equation for different cases of tyre response. Viscous damping is incorporated in the solution in an approximate way in Section 4. Boundary conditions of the contact edges are specified in Section 5. In Section 6, tyre and drum bearing reaction forces are determined. Section 7 is concerned with an illustrative numerical example. Some conclusions are drawn in Section 8.

2. DIFFERENTIAL EQUATION OF RING VIBRATIONS

The in-plane vibrations of the ring are normally described using two displacement components, i.e. its radial deflection, w, and the circumferential displacement, v. In the case of standing waves, the ring is exposed to a radial load. Since there is no circumferential load, circumferential displacement v is very small in comparison to w. Hence, it can be ignored in order to simplify the model.

The simplified differential equation for the ring in-plane vibrations can be deduced from a system of differential equations for a rotating cylindrical shell [24]. As a result, one obtains:

$$\frac{D}{R^4}\frac{\partial^4 w}{\partial \psi^4}-\frac{N_\psi}{R^2}\frac{\partial^2 w}{\partial \psi^2}+\left(\frac{K+N_\psi}{R^2}+k_r-m\Omega^2\right)w+c\frac{\partial w}{\partial t}+m\frac{\partial^2 w}{\partial t^2}=q_r\,, \tag{1}$$

where the particular symbols have the following meaning, Figure 1:

R – ring radius,

ψ – position angle,

D – bending stiffness,

K – tensional stiffness,

k_r – radial stiffness of the elastic foundation,

c – damping coefficient,

m – distributed mass per unit length,

Ω – ring rotation speed,

N_ψ – membrane force per unit length.

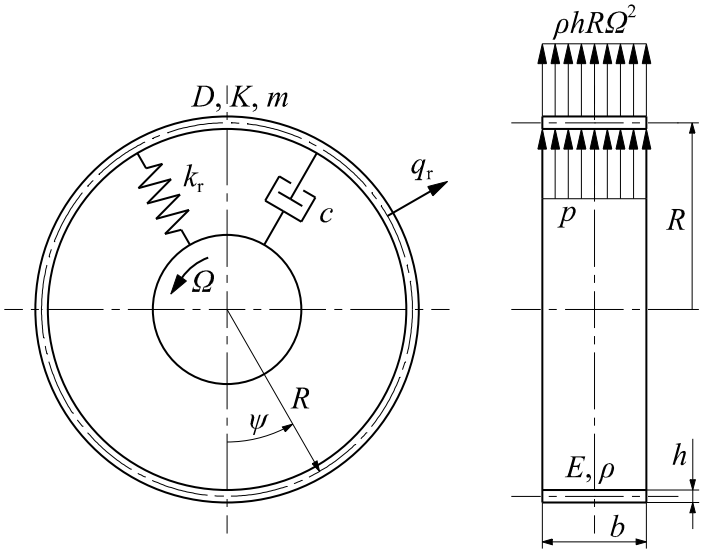

Fig. 1 *Particulars of ring model*

Furthermore,

$$K = EA, \quad A = bh,$$
$$D = EI, \quad I = \frac{bh^3}{12}, \tag{2}$$

where E is Young's modulus, A is the ring cross-section area, I is its moment of inertia, b is the ring width and h is the ring thickness, Figure 1.

The radial load consists of two parts, i.e. of a rotation-induced centrifugal load and a load due to the inflation pressure p:

$$\boldsymbol{q_r = mR\Omega^2 + pb}, \tag{3}$$

where $m = \rho h$, and ρ is mass density. Tyres are ordinarily pressurized in order to increase their stiffness which is realized through geometric stiffness. The pressure load increases the ring radius and induces the membrane force:

$$N_\psi = Rpb. \tag{4}$$

This pre-stressed state is used as the referent one for the vibration analysis and the pressure load is accordingly excluded from Eq. (1). As a result, Eq. (1) can be rewritten as:

$$\frac{D}{R^4}\frac{\partial^4 w}{\partial \psi^4}-\frac{q}{R}\frac{\partial^2 w}{\partial \psi^2}+\left(k+\frac{q}{R}-m\Omega^2\right)w+c\frac{\partial w}{\partial t}+m\frac{\partial^2 w}{\partial t^2}=mR\Omega^2. \tag{5}$$

Where:

$$q=pb,\quad k=\frac{K}{R^2}+k_r \tag{6}$$

and R is the radius of a pressurized ring.

Eq. (5) is specified in a rotating coordinate system fixed to the rotating ring. For a ground-fixed coordinate system, a new variable must be introduced:

$$\varphi=\Omega t+\psi. \tag{7}$$

The following relationships exist between these two coordinate systems:

$$\frac{\partial^n w}{\partial \psi^n}=\frac{d^n w}{d\varphi^n},\quad \frac{\partial^n w}{\partial t^n}=\Omega^n\frac{d^n w}{d\varphi^n}. \tag{8}$$

Substituting Eqs. (8) into Eq. (5) yields an ordinary differential equation for the description of standing waves:

$$\frac{D}{R^4}\frac{d^4 w}{d\varphi^4}+\left(m\Omega^2-\frac{q}{R}\right)\frac{d^2 w}{d\varphi^2}+c\Omega\frac{dw}{d\varphi}+\left(k+\frac{q}{R}-m\Omega^2\right)w=mR\Omega^2. \tag{9}$$

Eq. (9) is time-independent in the ground-fixed coordinate system, which is a characteristic feature of standing waves.

3. SOLUTION OF DIFFERENTIAL EQUATION

The particular solution of Eq. (9) reads:

$$w_0=\frac{mR\Omega^2}{k+\frac{q}{R}-m\Omega^2}. \tag{10}$$

It represents a uniform ring expansion due to the centrifugal load, i.e. an increase of the ring radius.

The homogeneous solution of Eq. (9) is assumed in an exponential form $w_\mathrm{h}=Ce^{r\varphi}$. The damping term in Eq. (9) is ignored for the time being in order to simplify the analysis. The characteristic equation of the differential Eq. (9) reads:

$$a_4r^4+a_2r^2+a_0=0, \tag{11}$$

where:

$$a_4=\frac{D}{R^4},\quad a_2=m\Omega^2-\frac{q}{R},\quad a_0=k+\frac{q}{R}-m\Omega^2. \tag{12}$$

The solutions of the bi-quadratic Eq. (11) are:

$$r_{1,2,3,4}=\pm\frac{1}{\sqrt{2a_4}}\sqrt{-a_2\pm\sqrt{a_2^2-4a_0a_4}}. \tag{13}$$

In its expanded form, Eq. (13) yields:

$$\boldsymbol{r_{1,2,3,4} = \pm\left(\frac{R^4}{2D}\right)^{\frac{1}{2}}\left\{\frac{q}{R} - m\Omega^2 \pm \left[\left(m\Omega^2 - \frac{q}{R}\right)^2 - \frac{4D}{R^4}\left(k + \frac{q}{R} - m\Omega^2\right)\right]^{\frac{1}{2}}\right\}^{\frac{1}{2}}} \tag{14}$$

The above roots are generally complex. They represent some characteristic values which depend on the ring rotation speed. The following five cases are considered:

Case 1, $\Omega = \Omega_{cr}$

If the term:

$$m\Omega^2 - \frac{q}{R} = 0, \tag{15}$$

the critical speed is obtained:

$$\Omega_{cr} = \sqrt{\frac{q}{mR}}. \tag{16}$$

Eq. (14) takes a specific form:

$$r_{1,2,3,4} = \pm(1 \pm i)\lambda, \quad \lambda = \sqrt[4]{\frac{R^4 k}{4D}} \tag{17}$$

and the homogeneous solution of Eq. (9) reads:

$$w_h = C_1 e^{\lambda\varphi} sin(\lambda\varphi) + C_2 e^{\lambda\varphi} cos(\lambda\varphi) + C_3 e^{-\lambda\varphi} sin(\lambda\varphi) + C_4 e^{-\lambda\varphi} cos(\lambda\varphi). \tag{18}$$

Expression (18) is similar to the deflection function of a beam on an elastic foundation.

Case 2, $\Omega = \Omega_{1,2}$

If the term in brackets of Eq. (14) is set to zero, i.e.

$$\boldsymbol{\left(\frac{q}{R} - m\Omega^2\right)^2 - \frac{4D}{R^4}\left(\frac{q}{R} - m\Omega^2\right) - \frac{4Dk}{R^4} = 0}, \tag{19}$$

the characteristic rotation speeds are obtained:

$$\Omega_1^2 = \frac{q}{mR} - \frac{2D}{mR^4}\left(\sqrt{1 + \frac{R^4 k}{D}} + 1\right), \quad \Omega_2^2 = \frac{q}{mR} + \frac{2D}{mR^4}\left(\sqrt{1 + \frac{R^4 k}{D}} - 1\right). \tag{20}$$

The first term in Eqs. (20) is the square of the critical speed Ω_{cr}, Eq. (16), while the second term represents a bifurcation due to the bending stiffness. Since Ω_1^2 cannot be negative, one obtains the minimum necessary pressure to fulfil this condition:

$$p_m = \frac{2D}{R^3 b}\left(\sqrt{1 + \frac{R^4 k}{D}} + 1\right). \tag{21}$$

Regarding Eq. (14), only two roots remain:

$$r_{1,2} = \pm\frac{1}{\sqrt{2}}\sqrt{\frac{R^4}{D}}\sqrt{\frac{q}{R} - m\Omega_{1,2}^2}. \tag{22}$$

If $\Omega = \Omega_1$ the roots are real:

$$r_{1,2} = \pm\alpha, \quad \alpha = \frac{1}{\sqrt{2}}\sqrt{\frac{R^4}{D}}\sqrt{\frac{q}{R} - m\Omega_1^2} \tag{23}$$

and the deflection function is exponential:

$$w_h = C_1 e^{\alpha\varphi} + C_2 e^{-\alpha\varphi}. \tag{24}$$

If $\Omega = \Omega_2$ the roots are imaginary:

$$r_{1,2} = \pm i\beta, \quad \beta = \frac{1}{\sqrt{2}}\sqrt{\frac{R^4}{D}}\sqrt{m\Omega_2^2 - \frac{q}{R}} \tag{25}$$

and the deflection function is harmonic:

$$w_h = C_1 \sin(\beta\varphi) + C_2 \cos(\beta\varphi). \tag{26}$$

Case 3, $\Omega < \Omega_1$

In this case, the roots presented by Eq. (14) are real:

$$r_{1,2} = \pm\alpha_1, \quad r_{3,4} = \pm\alpha_2 \tag{27}$$

and the deflection function is exponential:

$$w_h = C_1 e^{\alpha_1\varphi} + C_2 e^{-\alpha_1\varphi} + C_3 e^{\alpha_2\varphi} + C_4 e^{-\alpha_2\varphi}. \tag{28}$$

Case 4, $\Omega > \Omega_2$

In this case, the roots, Eq. (14), are imaginary:

$$r_{1,2} = \pm i\beta_1, \quad r_{3,4} = \pm i\beta_2 \tag{29}$$

and the deflection function is harmonic:

$$w_h = C_1 \sin(\beta_1\varphi) + C_2 \cos(\beta_1\varphi) + C_3 \sin(\beta_2\varphi) + C_4 \cos(\beta_2\varphi). \tag{30}$$

Case 5, $\Omega_1 < \Omega < \Omega_2$

In the central part of the rotation speed domain, the roots, Eq. (14), are complex:

$$r_{1,2,3,4} = \pm(\alpha \pm i\beta) \tag{31}$$

and one obtains exponential-harmonic deflection function:

$$w_h = C_1 e^{\alpha\varphi} \sin(\beta\varphi) + C_2 e^{\alpha\varphi} \cos(\beta\varphi) + C_3 e^{-\alpha\varphi} \sin(\beta\varphi) + C_4 e^{-\alpha\varphi} \cos(\beta\varphi). \tag{32}$$

It can be seen that rotation speeds Ω_1 and Ω_2 divide the speed domain into three parts with exponential response, combined exponential-harmonic response and pure harmonic response. For standing waves analysis, speed spans of harmonic response are of interest, i.e. $\Omega > \Omega_2$ (Case 4) and $\Omega_1 < \Omega < \Omega_2$ (Case 5). In the experimental investigation described in [7], it was observed that standing waves are highly damped and that there is no interaction between the contact edges. Hence, only the last terms in Eq. (32) are considered and one can write:

$$w_h = C_3 e^{-\alpha\varphi} \sin(\beta\varphi) + C_4 e^{-\alpha\varphi} \cos(\beta\varphi). \tag{33}$$

However, for response function in the $\Omega > \Omega_2$ range, Eq. (30), additional viscous damping has to be included. This is done in the next section.

4. INCORPORATION OF VISCOUS DAMPING

Let us now consider a homogeneous differential equation with viscous damping, i.e. Eq. (9). By setting $w_h = Ce^{r\varphi}$, the characteristic equation of Eq. (9) can be presented in the form:

$$r^4 + b_2 r^2 + b_1 r + b_0 = 0, \tag{34}$$

where:

$$\begin{aligned} b_2 &= \frac{R^4}{D}\left(m\Omega^2 - \frac{q}{R}\right), \quad b_1 = \frac{R^4}{D}c\Omega, \\ b_0 &= \frac{R^4}{D}\left(k + \frac{q}{R} - m\Omega^2\right) = \frac{R^4}{D}k - b_2. \end{aligned} \tag{35}$$

Solutions of Eq. (34) related to Case 4, $\Omega > \Omega_2$, are complex:

$$r_{1,2,3,4} = \pm\left(\tilde{\varepsilon} \pm i\beta\right), \tag{36}$$

where β is the argument of the undamped response function and $\tilde{\varepsilon}$ is the complex damping ratio. By substituting:

$$r = \tilde{\varepsilon} + i\beta \tag{37}$$

into Eq. (34) and omitting $\tilde{\varepsilon}$ terms of higher order (since $|\tilde{\varepsilon}| \ll \beta$), one obtains a linear algebraic equation:

$$\tilde{\varepsilon}\left[b_1 + 2i\beta\left(b_2 - 2\beta^2\right)\right] = -b_0 - ib_1\beta. \tag{38}$$

Taking into account $\tilde{\varepsilon} = \nu + \mathrm{i}\mu$, Eq. (38) is decomposed into its real and imaginary parts, i.e.

$$\begin{bmatrix} b_1 & -2\beta\left(b_2 - 2\beta^2\right) \\ 2\beta\left(b_2 - 2\beta^2\right) & b_1 \end{bmatrix} \begin{Bmatrix} \nu \\ \mu \end{Bmatrix} = \begin{Bmatrix} -b_0 \\ -b_1\beta \end{Bmatrix} \tag{39}$$

The solution of Eq. (39) reads:

$$\nu = \frac{D_\nu}{D_0}, \quad \mu = \frac{D_\mu}{D_0}, \tag{40}$$

where:

$$\begin{aligned} D_\nu &= -b_1\left[b_0 + 2\beta^2\left(b_2 - 2\beta^2\right)\right], \\ D_\mu &= \beta\left[-b_1^2 + 2b_0\left(b_2 - 2\beta^2\right)\right], \\ D_0 &= b_1^2 + 4\beta^2\left(b_2 - 2\beta^2\right)^2. \end{aligned} \tag{41}$$

Furthermore, the roots (36) can be written as:

$$r_{1,2,3,4} = \pm\left[\nu \pm i\left(\beta + \mu\right)\right]. \tag{42}$$

Normally $\mu \ll \beta$, therefore μ can be omitted in Eq. (42).

Generally speaking, an empirical value of the damping coefficient is ordinarily used for engineering structures, based on the response profile recorded in some experiments or in full scale measurements. Hence, if ν is given according to [7], c can be obtained from the first of Eqs. (40).

This equation can be presented in the form:

$$\nu b_1^2 + d_1 b_1 + \nu d_0 = 0, \tag{43}$$

where:

$$\begin{aligned} d_1 &= b_0 + 2\beta^2\left(b_2 - 2\beta^2\right), \\ d_0 &= 4\beta^2\left(b_2 - 2\beta^2\right)^2. \end{aligned} \tag{44}$$

Solution of Eq. (43) reads:

$$b_1^{(1,2)} = \frac{1}{2\nu}\left(-d_1 \pm \sqrt{d_1^2 - 4\nu^2 d_0}\right). \tag{45}$$

Since the second term in the square root in Eq. (45) is very small compared to the first one, it can be neglected and one can write:

$$b_1^{(1)} = 0, \quad b_1^{(2)} = -\frac{d_1}{\nu}. \tag{46}$$

Finally, setting $b_1 = b_1^{(2)}$, Eqs. (35) and (46), respectively, yields:

$$c \approx -\frac{D}{R^4 \Omega \nu}\left[b_0 + 2\beta^2\left(b_2 - 2\beta^2\right)\right]. \tag{47}$$

In the speed domain $\Omega > \Omega_2$, Case 4, the deflection is described by the harmonic solutions, Eq. (30). For each argument β_1 and β_2, accompanying damping ratios ν_1 and ν_2 are respectively obtained. Consequently, the deflection function is extended to:

$$w_h = C_1 e^{\nu_1 \varphi} \sin(\beta_1 \varphi) + C_2 e^{\nu_1 \varphi} \cos(\beta_1 \varphi) + C_3 e^{\nu_2 \varphi} \sin(\beta_2 \varphi) + C_4 e^{\nu_2 \varphi} \cos(\beta_2 \varphi). \tag{48}$$

Numerical examples show that the wave number $\beta_1 < \beta_2$, and damping ratios $\nu_1 < 0$ and $\nu_2 > 0$, respectively. Standing waves are generated at the trailing contact edge and gradually disappear when approaching the leading contact edge. Hence, for standing waves analysis in the range $\Omega > \Omega_2$, the first two terms of the deflection function from Eq. (48) are of interest. Setting $\nu_1 = -\nu$ and $\beta_1 = \beta$ yields:

$$w_h = C_1 e^{-\nu\varphi} \sin(\beta\varphi) + C_2 e^{-\nu\varphi} \cos(\beta\varphi). \tag{49}$$

5. BOUNDARY CONDITIONS

In order to simplify the determination of the boundary conditions for standing waves, a new variable $\vartheta = \varphi - \varphi_0$ is introduced as shown in Figure 2. In such a case, the complete deflection function, consisting of homogeneous and particular solutions, $w = w_h + w_0$, according to Eq. (49), reads:

$$w = C_1 e^{-\nu\vartheta} \sin(\beta\vartheta) + C_2 e^{-\nu\vartheta} \cos(\beta\vartheta) + w_0, \tag{50}$$

where w_0 is specified via Eq. (10). Rotation angle of standing waves takes the form:

$$\gamma = \frac{dw}{Rd\vartheta} = \frac{1}{R}\left\{C_1 e^{-\nu\vartheta}\left[-\nu \sin(\beta\vartheta) + \beta\cos(\beta\vartheta)\right] - C_2 e^{-\nu\vartheta}\left[\nu\cos(\beta\vartheta) + \beta\sin(\beta\vartheta)\right]\right\}. \tag{51}$$

At the trailing contact edge, the boundary conditions in Figure 2 read:

$$w(0)=w_0\,,\quad \gamma(0)=\gamma_0=\varphi_0+\eta_0\,. \tag{52}$$

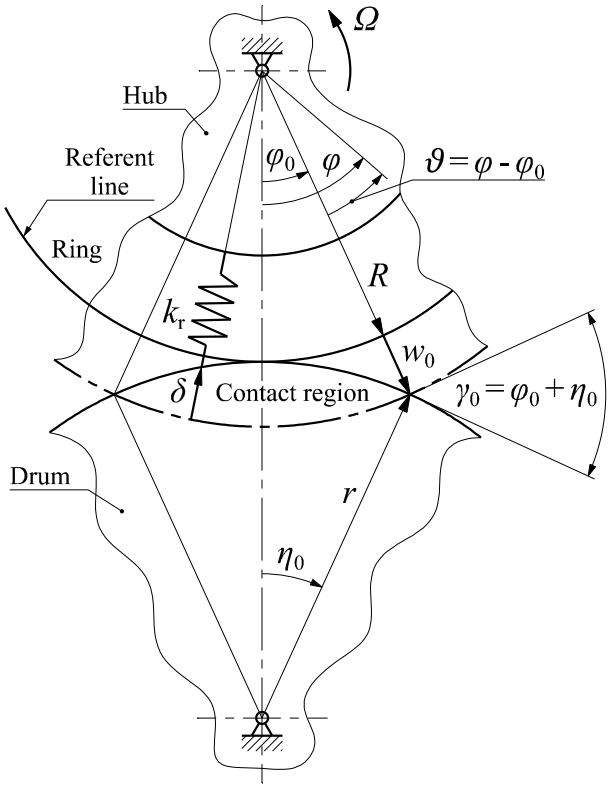

Fig. 2 *Tyre and drum particulars, and displacements at trailing contact edge, w_0 and γ_0*

Satisfying boundary conditions yields:

$$w=R\frac{\gamma_0}{\beta}e^{-\nu\vartheta}\sin(\beta\vartheta)+w_0\,. \tag{53}$$

Angles φ_0 and η_0 in Eq. (52) depend on the ring expansion due to the rotation, w_0. According to Figure 2, the following relationships between these two angles can be written:

$$\begin{aligned}(R+w_0)\cos\varphi_0+r\cos\eta_0&=R+r\,,\\(R+w_0)\sin\varphi_0&=r\sin\eta_0\,,\end{aligned} \tag{54}$$

where r is the radius of the drum. By employing the trigonometric identity $\sin\alpha=\sqrt{1-\cos^2\alpha}$, and by squaring and subtracting Eqs. (54), a linear equation is obtained:

$$\cos\eta_0=1-\frac{(2R+w_0)w_0}{2(R+r)r}. \tag{55}$$

The first unknown is obtained from the first of Eqs. (54), i.e.

$$\cos\varphi_0=\frac{2(R+r)R+(2R+w_0)w_0}{2(R+r)(R+w_0)}. \tag{56}$$

6. BEARING REACTION FORCES

Penetration of the rigid drum into the expanded tyre due to the centrifugal load causes an internal load within the contact region, $q_r = k_r\delta$, where δ is the tyre radial displacement, Figure 2. Reaction forces F are obtained by integrating this load along the tyre arch in the contact region:

$$F = k_r \int_{-\varphi_0}^{\varphi_0} \delta\left(R + w_0\right) d\varphi. \tag{57}$$

The above integral represents the Boolean intersect of the expanded tyre and the drum. It consists of the tyre and drum segments. Hence, one can write:

$$F = k_r \left[\left(R + w_0\right)^2 \left(\varphi_0 - sin\varphi_0 \, cos\varphi_0\right) + r^2 \left(\eta_0 - sin\eta_0 \, cos\eta_0\right) \right]. \tag{58}$$

7. NUMERICAL EXAMPLE

In order to illustrate the application of the proposed standing waves theory, the following parameters for the ring model of the tyre-drum system are used, according to [14], Figure 2: R = 0.3 m, r = 0.4 m, b = 0.2 m, h = 0.016 m, $E = 3 \cdot 10^7$ N/m^2, $\rho = 1.2 \cdot 10^3$ kg/m^3, $k_r = 0.97 \cdot 10^6$ N/m^2, $p = 0.2 \cdot 10^6$ N/m^2.

Based on the given data, some additional parameters are determined:

- ring cross-section area: $A = bh = 3.2 \cdot 10^{-3}$ m^2,
- moment of inertia of cross-section: $I = \dfrac{bh^3}{12} = 6.827 \cdot 10^{-8}$ m^4,
- tensile stiffness: $K = EA = 9.6 \cdot 10^4$ N,
- bending stiffness: $D = EI = 2.048$ N/m^2,
- distributed mass: $m = \rho A = 3.84$ kg/m,
- pressure load: $q = pb = 4 \cdot 10^4$ N/m,
- combined stiffness: $k = \dfrac{K}{R^2} + k_r = 203.66 \cdot 10^4$ N/m^2.

By employing Eqs. (16) and (20), the characteristic rotation speeds are shown in Figure 3 as functions of the inflation pressure. The critical membrane rotation speed Ω_{cr} is bifurcated into Ω_1 and Ω_2 due to the influence of the bending stiffness. At the given pressure of $p = 0.2 \cdot 10^6$ N/m^2, the characteristic rotation speeds take the following values:

$$\Omega_{cr} = 186.34 \text{ rad/s}, \; \Omega_1 = 150.83 \text{ rad/s}, \; \Omega_2 = 215.38 \text{ rad/s}.$$

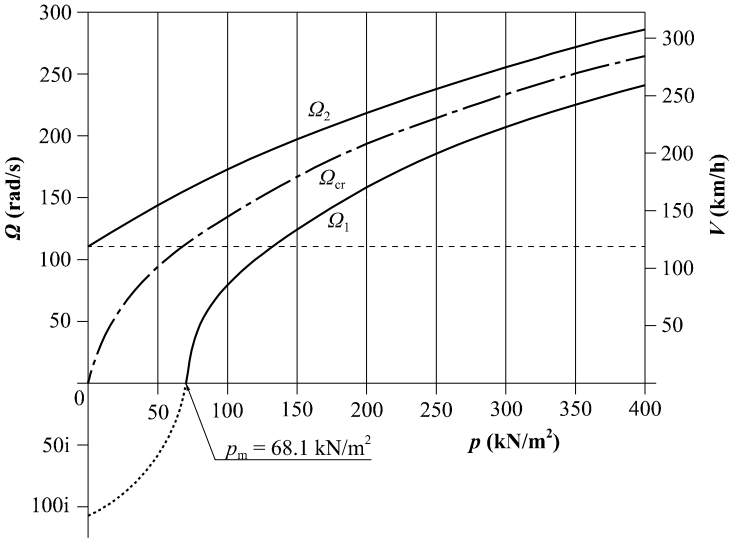

Fig. 3 *Characteristic tyre rotation speeds as functions of inflation pressure*

The diagrams of the standing wave number β, within domain $0 < \varphi < 2\pi$, and the amplitude exponent α, based on Eq. (14), for the given pressure are shown in Figure 4 as functions of the rotation speed. Parameter β is zero-valued at Ω_1, and then it increases up to Ω_2. Over Ω_2, it is bifurcated into two branches. A similar diagram, mirrored at Ω_{cr} is obtained for the amplitude exponent α. At Ω_{cr}, $\alpha = \beta = \lambda$. Parameters α and β can be expressed in terms of polar coordinates, $\alpha = r\cos\vartheta$ and $\beta = r\sin\vartheta$, where $r = \sqrt{\alpha^2 + \beta^2}$ and $\vartheta = arctg(\beta/\alpha)$. It is interesting that this radius is constant along the span $\Omega_1 - \Omega_2$, taking value 9.43, Figure 4.

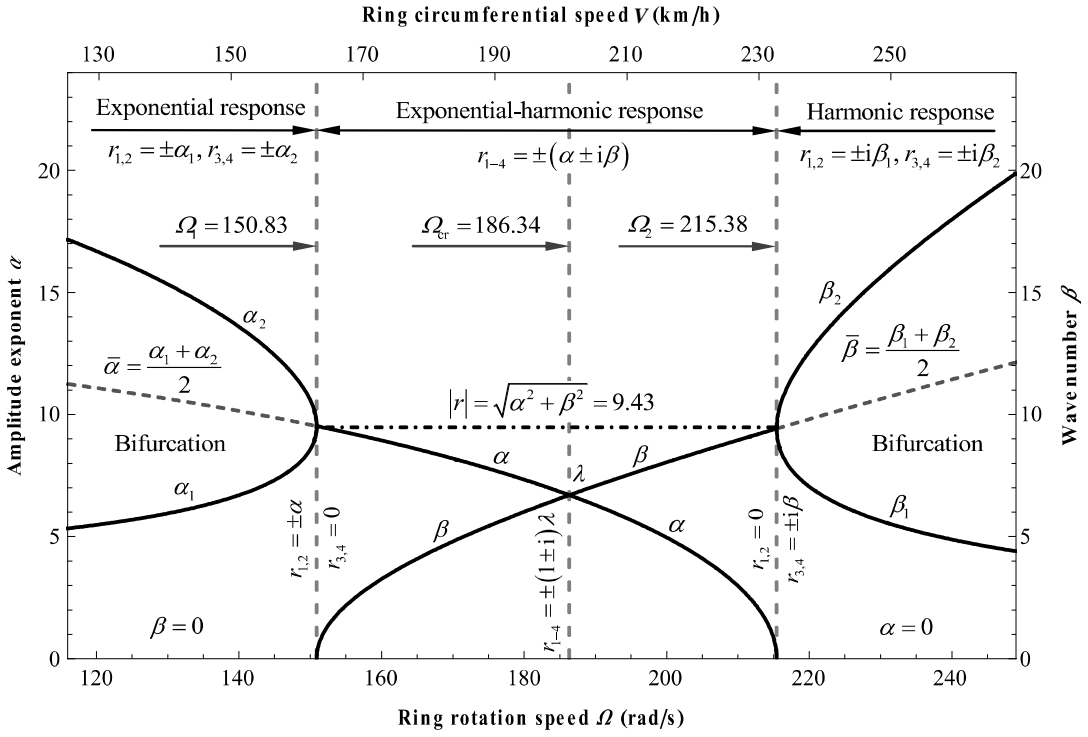

Fig. 4 *Roots of the characteristic equation of differential equation, p = 0.2·10⁶ N/m²*

Next, standing waves for $\Omega = \Omega_{cr}$ are determined. By employing Eqs. (10), (17), (55) and (56) one finds: $w_0 = 0.0196\ m$, $\lambda = 6.70$, $\varphi_0 = 0.2646\ rad$, $\eta_0 = 0.2111\ rad$, $\gamma_0 = 0.4757\ rad$. The standing waves amplitude is determined via Eq. (53), i.e. $w_a = R\gamma_0/\lambda = 0.0213\ m$. The standing waves are shown in Figure 5. This case is actually a linear static problem with a quasi-dynamic centrifugal load. Since the boundary conditions have to be satisfied at both contact edges, the standing waves are shown on both sides. Due to the very large amplitude decrement, $\alpha = \beta = \lambda$, the standing waves disappear within the first period. Such a response has been observed in experiments and described as a ripple, [7].

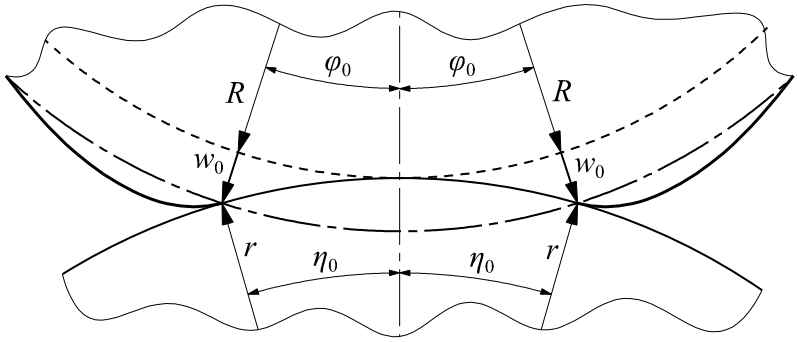

Fig. 5 *Tyre standing waves, $\Omega_{cr} = 186.34$ rad/s, V = 201 km/h*

Ω_2 is another interesting rotation speed for the determination of standing waves. In this case one finds: $w_0 = 0.031\ m$, $\alpha = 0$, $\beta = 9.43$, $\varphi_0 = 0.3221\ rad$, $\eta_0 = 0.2651\ rad$, $\gamma_0 = 0.5872\ rad$, $w_a = 0.0187\ m$. Since the amplitude decrement $\alpha = 0$, a damping ratio of $\nu = 0.7$ is used. This corresponds to the damping coefficient determined by Eq. (47), $c = 1.321 \cdot 10^4\ Ns/m^2$. Standing waves are shown in Figure 6. Ripple is also included in the figure.

Furthermore, the standing waves are determined for $\Omega = 230\ rad/s$ which belongs to the bifurcation domain, Figure 4. The following parameters are determined: $w_0 = 0.031\ m$, $\beta_1 = 5.64$, $\beta_2 = 15.63$, $\varphi_0 = 0.3211$ rad, $\eta_0 = 0.2651\ rad$, $\gamma_0 = 0.5872\ rad$, $w_a = 0.0312\ m$. The same damping ratio is used as in the previous case for the lower branch, i.e. $\nu_1 = 0.7$. The damping coefficient obtained via Eq. (47) is $c = 3.334 \cdot 10^4\ Ns/m^2$. By using known values of c and β_2, the following damping ratio is obtained for the upper branch: $\nu_2 = 3.016$, which causes a spreading of the deflection function. Standing waves for case ν_1 and β_1 are shown in Figure 7. It is obvious that the number of waves is smaller than in the previous case, Figure 6. The standing waves profile is similar to those observed in the experiments, [7], [23]. They attenuate significantly before reaching the leading edge of the contact region.

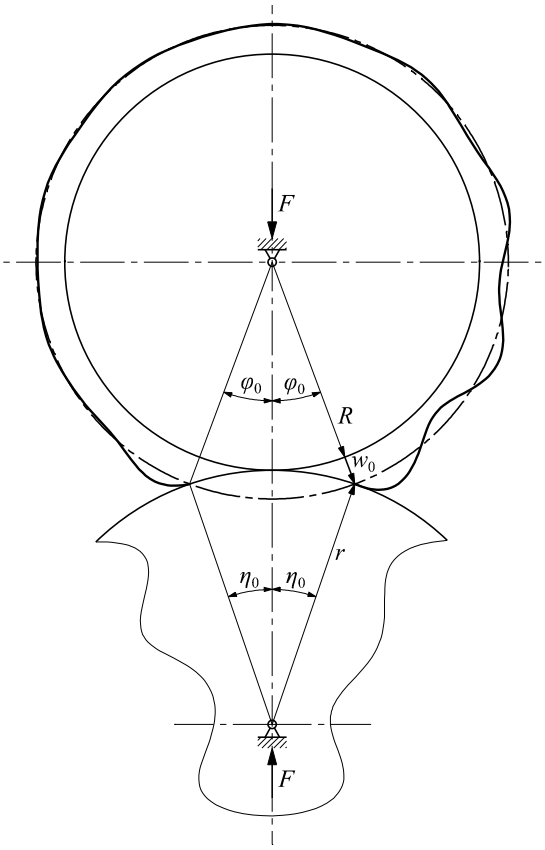

Fig. 6 *Tyre standing waves, Ω_2 = 215.38 rad/s, V = 233 km/h*

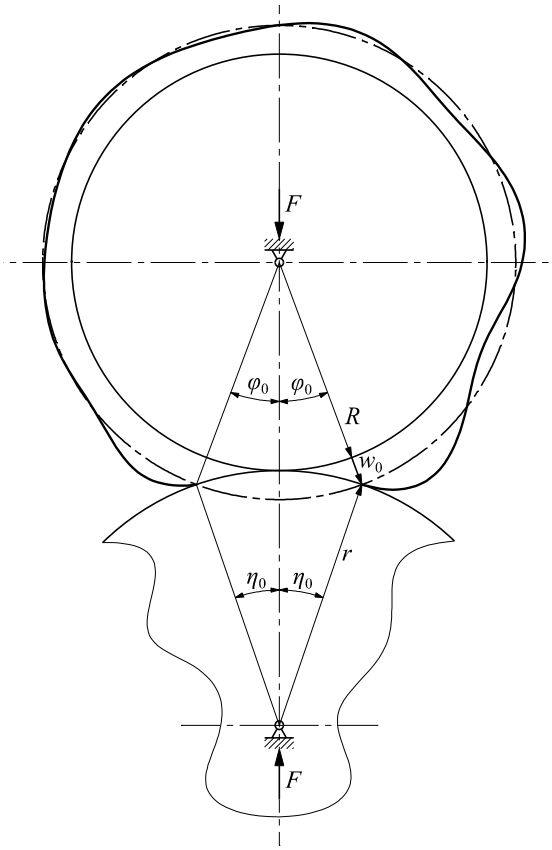

Fig. 7 *Tyre standing waves, Ω = 230 rad/s, V = 248 km/h*

In addition, a diagram of the bearing reaction force, F, as a function of the tyre expansion due to the centrifugal load is shown in Figure 8. The diagram is very similar to the experimental one, [23]. In Figure 9, diagrams of both the ring expansion and the bearing reaction force as functions of the rotation speed are shown. Also, the tyre peripheral velocity $V = R\Omega$, is included in order to indicate the vehicle speed.

In the case of a balloon tyre, the bending stiffness is negligible. The generation of standing waves has been investigated by measurements on a test bed and analysed via a simplified ring model, [7]. A sophisticated ring mathematical model based on the same experiment is presented in [25]. Roots of the characteristic equation of the governing differential equation of motion are shown in Figure 10. Comparing Figure 4 for $D > 0$ and Figure 10 for $D = 0$, it is obvious that by reducing the bending stiffness, the characteristic rotation speeds Ω_1 and Ω_2 approach Ω_{cr} for the case $D = 0$, while the roots $\pm\alpha$ and $\pm\beta$ approach infinity.

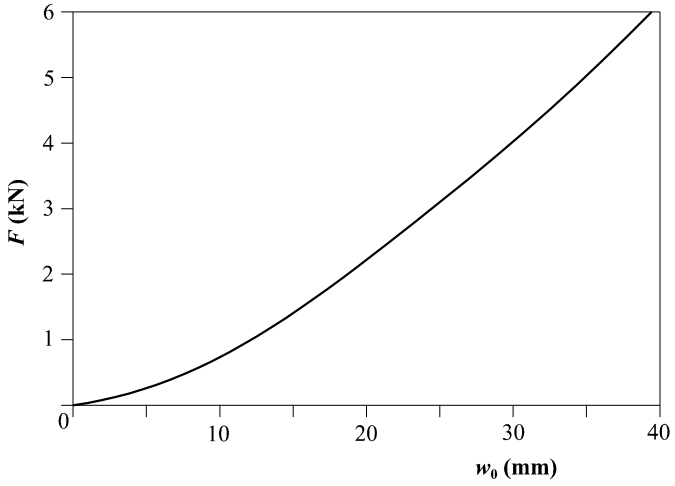

Fig. 8 *Bearing reaction force as a function of tyre expansion due to rotation*

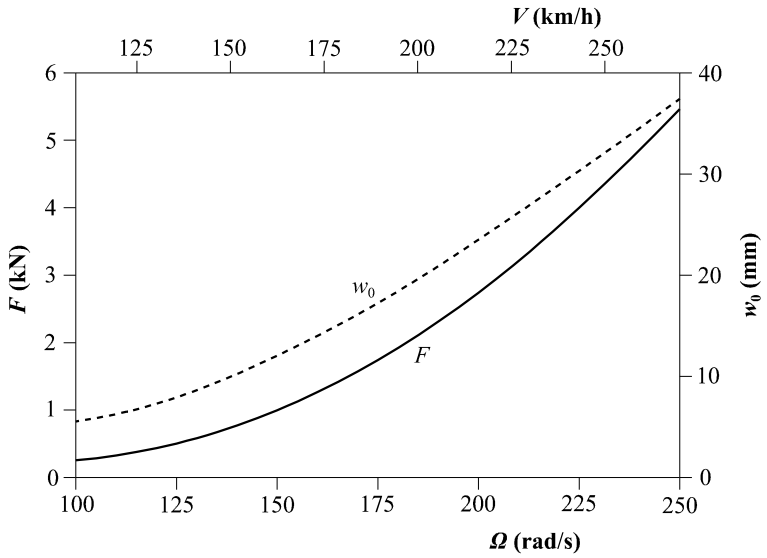

Fig. 9 *Bearing reaction force and tyre expansion as functions of rotation speed*

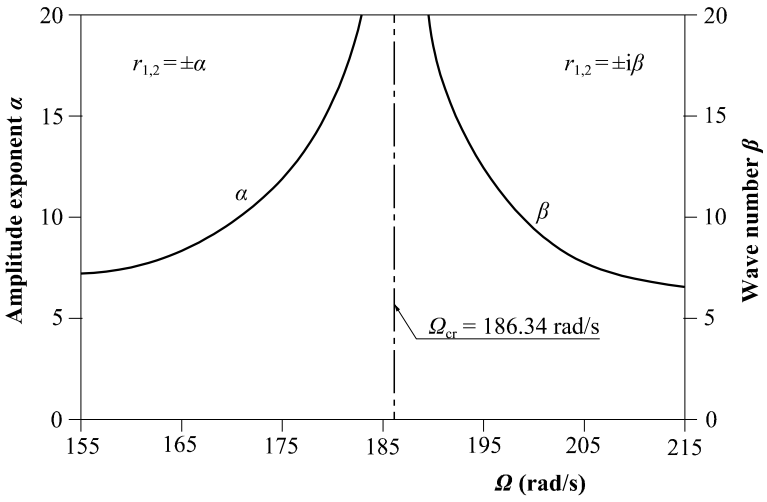

Fig. 10 *Roots of characteristic equation via neglecting the bending stiffness, D = 0 (balloon)*

8. CONCLUSION

In the relevant literature, the generation of standing waves has been related to a shock at the leading contact edge, resonance with natural vibrations and a loss of dynamic stability. In this paper, it is shown that the generation of standing waves starts when the tensional force due to the tyre rotation overcomes the inflation pressure tensional force. The equilibrium of these forces defines the critical rotation speed. In the case of a membrane structure without bending stiffness (e.g. balloon tyre), the development of standing waves when the structure rotates at a speed higher than critical is very fast. In real tyres with inherent bending stiffness, the generation of standing waves is slow up to the common membrane and bending critical speed. After that, the number of standing waves is reduced and their amplitude is increased. The diagram of roots of the characteristic equation shown in Figure 4 may be useful to follow the development of standing waves.

Due to the tyre rotation and induced centrifugal load, the tyre radius is increased. The constant distance between the tyre and the drum shafts defines the contact region and boundary conditions for standing waves. Bearing reaction forces depend on both the contact area and the radial stiffness. This is a linear boundary problem. Damping plays an important role in the over-critical range and it is included in the response function in an approximate but realistic way.

The presented theory sheds more light onto understanding the physical mechanism responsible for the generation of tyre standing waves and their behaviour for the different values of imposed tyre parameters. The theory can be adapted to the problem of the generation of standing waves in a tyre driven by the flat moving strap. This is actually a special case of a drum with an infinite radius and zero rotational speed, giving finite peripherical velocity ($V = R\Omega$). Moreover, by following the 2D theory, the problem of the standing wave generation in a tyre rolling along the road can be mathematically modelled. This is a subject of further investigation.

9. ACKNOWLEDGEMENT

This work has been supported by the Croatian Science Foundation under the project IP-2019-04-5402.

10. REFERENCES

[1] Ames, W.F., Waves in tires: Part I: Literature review on traveling waves, *Textile Research Journal* 40(6) (1970) 498-503. https://doi.org/10.1177/004051757004000602

[2] Huang, S.C., Soedel, W., Response of rotating rings to harmonic and periodic loading and comparison with the inverted problem, *Journal of Sound and Vibration* 118(2) (1987) 253-270. https://doi.org/10.1016/0022-460X(87)90524-4

[3] Huang, S.C., The vibration of rolling tyres in ground contact, *International Journal of Vehicle Design* 13(1) (1992) 78-95.

[4] Huang, S.C., Su, C.K., In-plane dynamics of tires on the road based on an experimentally verified rolling ring model, *Vehicle System Dynamics* 21(1) (1992) 247-267.
https://doi.org/10.1080/00423119208969011

[5] Stutts, D.S., Soedel, W., A simplified dynamic model of the effect of internal damping on the rolling resistance in pneumatic tires, *Journal of Sound and Vibration* 155(1) (1992) 153-164. https://doi.org/10.1016/0022-460X(92)90652-E

[6] Lindsley, N.J., Cusumano, J.P., Critical Speed Analysis of a Non-Linear Strain Ring Dynamical Model for Aircraft Tires, *SAE Technical Paper* (1993) 932580.

https://doi.org/10.4271/932580

[7] Chatterjee, A., Cusumano, J.P., Zolock, J.D., On contact-induced standing waves in rotating tires: Experiment and theory, *Journal of Sound and Vibration* 227(5) (1999) 1049-1081.

https://doi.org/10.1006/jsvi.1999.2395

[8] Kung, L.E., Soedel, W., Yang, T.Y., Free vibration of a pneumatic tire-wheel unit using a ring on an elastic foundation and a finite element model, *Journal of Sound and Vibration* 107(2) (1986) 181-194. https://doi.org/10.1016/0022-460X(86)90231-2

[9] Ji, X.W., Gao, Y.M., Qiu, X.D., Li, Y.D., Zhuang, J.D., The dynamic stiffness and damping characteristics of the tire, *Automotive Engineering* 16(5) (1994) 315-320.

[10] Chang, Y.P., El-Gindy, M., Streit, D.A., Influence of tyre loading and inflation pressure on standing waves phenomenon using PAM-SHOCK, *International Journal of Heavy Vehicle Systems* 10(1/2) (2003) 86-111. https://doi.org/10.1504/IJHVS.2003.002436

[11] Vinesse, E., Nicollet, H., Surface waves on the rotating tyre: An application of functional analysis, *Journal of Sound and Vibration* 126(1) (1988) 85-96.

https://doi.org/10.1016/0022-460X(88)90400-2

[12] Lecomte, C., Graham, W.R., Dale, M., A shell model for tyre belt vibrations, *Journal of Sound and Vibration* 329(10) (2010) 1717–1742.

https://doi.org/10.1016/j.jsv.2009.11.022

[13] Soedel, W., On the dynamic response of rolling tires according to thin shell approximations, *Journal of Sound and Vibration* 41(2) (1975) 233-246.

https://doi.org/10.1016/S0022-460X(75)80099-X

[14] Krylov, V.V., Gilbert, O., On the theory of standing waves in tyres at high vehicle speeds, *Journal of Sound and Vibration* 329(21) (2010) 4398-4408.

https://doi.org/10.1016/j.jsv.2010.05.001

[15] Padovan, J., On viscoelasticity and standing waves in tires, *Tire Science and Technology* 4(4) (1976) 233-246. https://doi.org/10.2346/1.2167224

[16] Padovan, J., On standing waves in tires, *Tire Science and Technology* 5(2) (1977) 83-101.

https://doi.org/10.2346/1.2167234

[17] Kennedy, R., Padovan, J., Finite element analysis of a steady-state rotating tire subjected to point load or ground contact, *Tire Science and Technology* 15(4) (1987) 243-260.

https://doi.org/10.2346/1.2148792

[18] Padovan, J., Kazempour, A., Tabaddor, F., Brockman, B., Evaluation of critical speeds in high speed aircraft tires, *SAE Technical Paper* (1989) 892349.

https://doi.org/10.4271/892349

[19] Brockman, R.A., Champion, J.H., Medzorian, J.P., Finite element analysis of tire critical speeds, *Computers & Structures* 43(3) (1992) 581-593.

https://doi.org/10.1016/0045-7949(92)90290-G

[20] Cho, J.R., Kim, K.W., Jeong, H.S., Numerical investigation of tire standing wave using 3-D patterned tire model, *Journal of Sound and Vibration* 305(4–5) (2007) 795-807.

https://doi.org/10.1016/j.jsv.2007.04.049

[21] Ozaki, S., Kondo, W., Finite element analysis of tire traveling performance using anisotropic frictional interaction model, *Journal of Terramechanics* 64 (2016) 1-9.

https://doi.org/10.1016/j.jterra.2015.12.001

[22] Mashadi, B., Ebrahimi-Nejad, S., Abbaspour, M., A rolling resistance estimate using nonlinear finite element numerical analysis of a full three-dimensional tyre model, *Proceedings of the Institution of Mechanical Engineers, Part D: Journal of Automobile Engineerin*g 233(1) (2019) 147-160. https://doi.org/10.1177/0954407018802733

[23] Zhou, S.T., Du, M., Sun, P.F., Chiu, Y.J., Fan, J.W., Experimental and theoretical analysis of high-speed radial tire standing waves, *Journal of the Brazilian Society of Mechanical Sciences and Engineering* 42 (2020) 200.

https://doi.org/10.1007/s40430-020-2253-2

[24] Senjanović, I., Ćatipović, I., Alujević, N., Vladimir, N., Čakmak, D., A finite strip for the vibration analysis of rotating cylindrical shells, *Thin-Walled Structures* 122 (2018) 158-172. https://doi.org/10.1016/j.tws.2017.10.017

[25] Senjanović, I., Čakmak, D., Alujević, N., Ćatipović, I., Vladimir, N., Mathematical model for simulation of contact-induced standing waves in tyres by rotating ring based on experiment, *International Journal for Engineering Modelling* 35 (2022) 2, 91-121.

https://doi.org/10.31534/engmod.2022.2.ri.06m